

## TRANSPORT AND MIXING OF ATMOSPHERIC POLLUTANTS

Peter Haynes

*Department of Applied Mathematics and Theoretical Physics  
University of Cambridge  
Wilberforce Road, Cambridge, CB3 0WA, UK  
phh@damtp.cam.ac.uk*

It is now realised that air quality is determined not only by local emissions and local meteorology, but also by long-range atmospheric transport of chemical species from emission regions that may be thousands of kilometres from the region of interest.

Predicting and understanding air quality requires consideration of many different processes, including emissions, boundary layer physics, chemical reactions and interactions with clouds and particles. These lecture notes focus on the role of atmospheric transport and mixing, emphasising the fundamental ideas and describing relevant mathematical models. In many parts of the atmosphere large-scale quasi-horizontal flow appears to play the dominant role in transport and in the stirring process that leads ultimately to true (molecular) mixing at very small scales. This means that calculations based on large-scale meteorological datasets can give valuable quantitative information on transport. To make local predictions requires more detailed information on transport, e.g. from regional-scale models.

### Contents

1	Motivation	2
2	Transport and mixing in the atmosphere	4
3	Fundamentals of transport and mixing	7
3.1	Definitions	7
3.2	Evolution equations	8
3.3	Stretching in linear flows	9
3.4	The relation between stretching and mixing	13
3.5	'Type I' and 'Type II' flows	14

3.6	Stirring and transport in quasi-two-dimensional flows	17
4	Modelling approaches	19
5	Examples	23
5.1	The 2000 ACTO campaign – combining chemical measurements and backward trajectory calculations (Methven et al 2003)	23
5.2	'Around the world in 17 days' – transport of smoke from Russian forest fires (Damoah et al 2004)'	28
5.3	'Observational and modeling analysis of a severe air pollution episode in western Hong Kong' (Fung et al 2005)	32
6	Conclusion	35
	References	36

## 1. Motivation

The effect of pollution on air quality has been a concern for at least the last 150 years or so and in some cases for longer. Poor air quality originally resulted primarily from coal burning, both domestic and industrial. By the 1950s a distinct problem of photochemical smog resulting primarily from car exhausts had been identified. This was particularly serious in large cities such as Los Angeles where topography favoured the trapping (and subsequent photochemical evolution) of polluted air. In such cases the problem is essentially one of local emissions in a given urban area (perhaps a very large urban area such as the Los Angeles basin) leading to an adverse effect on air quality in that same area.

However more recently the non-local effects of air pollution have been recognised. One example is that of acid rain where the effect of emission of sulphur compounds as part of coal burning is felt 100s of kilometers away through rainfall that is significantly more acidic than normal, with adverse effects on vegetation and on soil and freshwater ecosystems. Another example is that of low-level ozone, which results from emissions of nitrogen oxides and hydrocarbons (known as ozone precursors). Low-level ozone is potentially harmful to human health and to agriculture [1, 2]. Ozone concentrations in emission regions are sometimes relatively low in emissions regions, e.g. in the centre of cities, because high concentrations of nitrogen oxides limit ozone concentrations. However away from these regions, e.g. in suburbs and surrounding rural areas, nitrogen oxide concentrations decrease and ozone concentrations therefore increase. (A corollary is that reduction of nitrogen oxide emissions in city centres, e.g. through installation of catalytic convertors on car exhausts, has actually increased local ozone concentrations.) It has been recognised for some time that since, away from the Earth's surface, the lifetime of tropospheric ozone is relatively long

(perhaps 20 days or more) ozone concentrations in Europe, for example, are determined not locally, but by precursor emissions over a broad continental region and efforts to limit or even reduce ozone concentrations have had to focus on continent-wide emissions of the ozone precursors. Indeed it is now clear that local concentrations of ozone are affected by intercontinental transport e.g. [3] and the hemispheric, or indeed global, aspects of air quality are being now being recognised. Ensuring air quality standards are met therefore requires not just regional but global policies on emissions [4].

It has also been recognised that emissions from non-industrial sources such as agricultural waste burning and forest fires make a significant contribution to gases such as carbon monoxide. Again since the lifetime of carbon monoxide and in turn can significantly affect air quality in populated regions. In South East Asia such biomass burning has had a large-scale effect on air quality, particularly in during 1997, but also in several subsequent years. with the effects, being felt well over 1000km away from the primary burning regions. The problems experienced in 1997 and subsequently have prompted the formulation of an ASEAN agreement on Transboundary Haze Pollution.

Quantitative prediction of air quality is therefore now seen to require not only modelling of local emission and transport, but also transport on a regional and indeed even global scale. Of course incorporation of processes on this range of scales may not be possible in a single numerical model, and specific problems will require a specific focus. But an effective overall scientific perspective does need to take account of the global as well as local aspects of the problem.

The recognition that local, regional and hemispheric scale processes are relevant to air quality broadens the range of physical processes that are relevant and that must be incorporated in predictive numerical models. Such models must represent emissions, chemical evolution and transport and mixing by the atmospheric flow. Numerical modelling is a well-developed field and many sophisticated approaches have been devised to represent the effects of different processes. The purpose of these notes is not to describe state-of-the-art numerical modelling, but to set out some of the basis physical processes of atmospheric transport and mixing that must be represented in models. A much broader review of atmospheric composition change, its implications for global and regional air quality and modelling approaches is provided in [5].

## 2. Transport and mixing in the atmosphere

There is no space in this article for detailed discussion of the dynamics of the atmospheric flow, which determines the transport and mixing properties. This is well discussed elsewhere in textbooks such as those by (in increasing levels of sophistication and detail) Houghton [6], Holton [7] and Vallis [8]. But a very brief summary of some key points is given below.

A major role in determining the nature of the atmospheric flow is played by stable density stratification, which tends to inhibit vertical motion. The primary physical quantity determining density variations is temperature, however density variations associated with pressure also need to be taken into account and it turns out that the most appropriate density variable is potential temperature,  $\theta = T(p/p_*)^{-\kappa}$  where  $T$  is temperature,  $p$  is pressure,  $p_*$  a constant reference pressure and  $\kappa$  is a constant, equal to  $2/7$ .  $\theta$  is conserved by an air parcel in adiabatic motion – it therefore allows assessment of the effects of vertical displacements. If  $\theta$  increases upwards then an air parcel that is displaced upwards will find itself denser than its surroundings and will therefore tend to return to its original level – i.e. the density stratification is stable. On the other hand if  $\theta$  decreases upwards then an air parcel displaced upwards will find itself lighter than its surroundings and will tend to move further upwards – i.e. the density stratification is unstable. More precisely an appropriate measure of stability is the square of the buoyancy frequency  $(g/\theta)(d\theta/dz) = (g/T)(dT/dz + \kappa g/R)$  where  $g$  is the gravitational acceleration,  $R$  is the gas constant and the second term in the sum follows from the hydrostatic equation and the gas law. If  $dT/dz + \kappa g/R$  is positive then the stratification is stable and if it is negative the stratification is unstable.

This dependence of stability on vertical temperature gradient motivates the conventional division of the atmosphere into layers according to the vertical temperature gradient. In the *troposphere* (the lowest 10 km or so of the atmosphere) the temperature decreases with height and whilst the associated density stratification is stable (since  $-dT/dz < \kappa g/R$ ), the stability is relatively weak. In the *stratosphere* (roughly 10-50km) the temperature is constant with height or increases with height and the stability is much stronger than in the troposphere. The dynamical differences between troposphere and stratosphere, due to the differing stability, are mirrored in chemical differences with, for example, water vapour concentrations in the troposphere being much higher than in the stratosphere and, conversely, ozone concentrations being much lower. (The explanation lies in transport

and mixing together with the different sources and sinks of different chemical species.) The transition from troposphere to stratosphere as conventionally been viewed as sharp and the location of the transition is called *tropopause*. However for many purposes it is better to consider the transition as taking place over a *tropopause layer* of finite thickness.

The stabilisation due to density stratification (and to some extent rotation) mean that three-dimensional turbulence (i.e. the sort of turbulence that would be observed in a wind tunnel, or in a strongly stirred laboratory tank) is confined to relatively localised regions of the atmosphere. In the troposphere these regions include the atmospheric boundary layer (the lowest kilometer or so of the atmosphere where dynamical effects of direct contact with the Earth's surface overcome the stabilisation) and to convective clouds (where the stabilisation is overcome by dynamical effects of moist processes such as condensation). However, even in the tropics, where moist dynamics is most important, convective clouds fill a relatively small fraction of the total area. Elsewhere in the troposphere and stratosphere there are localised regions of turbulence resulting from dynamical instabilities such as the breaking of inertia-gravity waves. Even in the troposphere, the time scale on which air masses encounter these turbulent regions might be relatively long – several days or more. Evidence for this comes, for example, from the observations of thin layers with a distinct chemical signature, which are likely to have been transported thousands of kilometers from their formation regions [9].

In considering flow outside of regions of three-dimensional turbulence potential temperature  $\theta$  (which increases upwards) is a useful vertical coordinate. Processes which change the potential temperature of an air parcel are relatively weak (molecular dissipation in 3-D turbulence, radiative transfer) and therefore to a reasonable approximation – on a time scale of a few days in the troposphere and longer in the stratosphere – air parcels move along surfaces of constant  $\theta$ . The implication is that air parcels can move rapidly along  $\theta$  surfaces, but only slowly across them.

Figure 1 shows longitudinally averaged temperature and potential temperature ( $\theta$ ) fields for the atmosphere, which gives a good impression of the typical configuration of the  $\theta$ -surfaces in a latitude-height cross section. Note that in the weakly stable troposphere the  $\theta$ -surfaces are relatively widely separated in the vertical, whilst in the strongly stable stratosphere they are closer together. In the extratropical troposphere the  $\theta$ -surfaces slope strongly, indicating a rapid route for transport from the surface (or the boundary layer) to the upper troposphere, or vice versa. This is an

important aspect of the intercontinental transport of pollution mentioned in §1. The tropopause is marked in Figure 1 by the thick curve. Note that outside of the tropics the  $\theta$ -surfaces, e.g. the 320K surface, cut across the tropopause implying the possibility of rapid transport from the stratosphere to the troposphere and even to the surface and, again, vice versa. The part of the stratosphere, marked as shaded in 1, that is accessible from the troposphere via  $\theta$  surfaces is sometimes called the *lowermost stratosphere* [10]. If there were unrestricted rapid motion along  $\theta$ -surfaces then one might expect significant differences between this part of the stratosphere and that above. The differences are not so great, otherwise the shaded region might have been historically identified as troposphere rather than stratosphere. This illustrates the important point that whilst rapid transport along  $\theta$ -surfaces is possible, it is not guaranteed. It turns out, for example, that transport along the 320K  $\theta$ -surface is relatively inhibited in the region of the tropopause (and if it was not then the dynamical and chemical contrast between troposphere and stratosphere on that  $\theta$ -surface would disappear). This inhibition of transport is consistent with the presence of the subtropical jet in this region in each hemisphere, i.e. at 30-40 degrees of latitude and between 8-12 km in altitude. (See further comments in §3.6.)

The processes that are involved in quasi-horizontal transport along  $\theta$ -surfaces include synoptic-scale weather systems, larger scale 'planetary' waves that modulate the circulation on scales of thousands of kilometers and, in the tropics, large-scale circulations associated with features such as monsoons, driven by spatial variations in sea-surface temperatures and by heating contrasts between land and ocean. All of these flows vary strongly in longitude. Local variations are, of course, important in determining local chemical distributions, but it is also the case that the averaged effect of the longitudinally varying flows needs to be taken account in explaining the height-latitude variation of the distributions of different chemical species. The longitudinally varying flow has a dual character, with some aspects of its behaviour appearing organised and wave-like and other aspects exhibiting considerable nonlinearity and randomness. In the latter respect the flow might therefore be regarded as a kind of turbulence, closely related to the two-dimensional turbulence studied in idealised numerical simulations and in laboratory experiments where there is rapid rotation or strong density stratification (and very different from three-dimensional turbulence). (See e.g. Chapters 8 and 9 of the book by Vallis [8].)

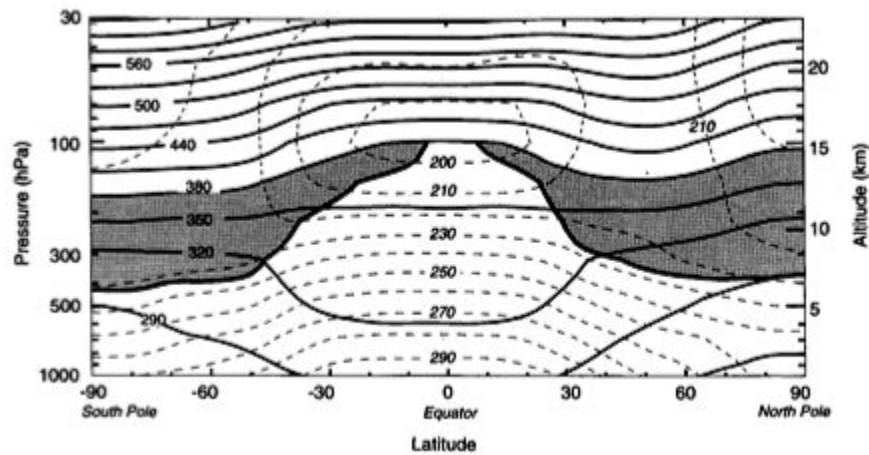


Fig. 1. Reproduced from [10]. Latitude-altitude cross section for January 1993 showing longitudinally averaged potential temperature ( $\theta$ ) (solid contour) and temperature (dashed contours). Contours, e.g.  $\theta$ -contours, in this cross-section correspond to surfaces in the 3-D atmosphere. The heavy solid contour (cut off at the 380K  $\theta$  contour) denotes the tropopause defined as the 2-PVU potential vorticity contour. (See [10] for more details.) Shaded areas denote the 'lowermost stratosphere', being the part of the stratosphere which contains  $\theta$ -surfaces which enter the troposphere. Data are from United Kingdom Meteorological Office analyses. Copyright 2003 American Geophysical Union. Reproduced by permission of American Geophysical Union.

### 3. Fundamentals of transport and mixing

#### 3.1. Definitions

The atmospheric flow (or any other flow) affects the distribution of chemical species through at least three distinct processes. Firstly it moves chemical species away from their source regions, where they might be emitted by natural processes or by human activity or produced in-situ by suitable chemical reactions, e.g. photochemical production, to other regions where they might be detected by suitable measurement, or indeed they might be destroyed by chemical reaction or absorbed at the land or sea surface or onto cloud particles. This process by which chemical species are carried away from source regions to some other part of the flow is called *transport*. Unless the flow is uniform in space, it not only carries chemical species from one location to another, but it also distorts the spatial structure of chemical concentration fields, typically making the spatial structure more complicated by drawing out the concentration field of the chemical species

into thin filaments or sheets. This process of distortion is called *stirring*. Ultimately molecular diffusion acts to homogenise chemical concentration fields. This latter process is called *mixing*. Note that if two chemical species A and B, which potentially react together, are emitted in different regions then the final state of mixing is essential for the reaction to proceed. Stirring may lead to thin interleaved filaments or sheets containing either A or B, but the molecules of A or B are separate. It is only when mixing occurs at the molecular level, through the action of molecular diffusion, that the reaction may proceed.

[Note that in some descriptions the term 'mixing' is used without the requirement for molecular diffusion – e.g. a flow may be described as strongly mixing if it is strongly stirring, since only a small molecular diffusion is needed to change from a 'stirred' state to a 'mixed' state. But in the chemical context the distinction is very important.]

### 3.2. Evolution equations

In considering transport, stirring and mixing it can be useful to consider the evolution in time  $t$  of either the position  $\mathbf{X}(t)$  of a marked particle or the concentration field  $\chi(\mathbf{x}, t)$  of a chemical species, with  $\mathbf{x}$  being position. Given a velocity field  $\mathbf{u}(\mathbf{x}, t)$  the position of a marked particle evolves according to

$$\frac{d\mathbf{X}}{dt} = \mathbf{u}(\mathbf{X}, t), \quad (3.1)$$

and the concentration field evolves according to

$$\frac{D\chi}{Dt} = \frac{\partial\chi}{\partial t} + \mathbf{u} \cdot \nabla\chi = \kappa \nabla^2 \chi \quad (3.2)$$

(Estimate)       $\frac{\chi U}{L}$        $\frac{\kappa \chi}{L^2}$

where  $\kappa$  is the molecular diffusivity. The operator  $D/Dt = \partial/\partial t + \mathbf{u} \cdot \nabla$  is called the advective derivative and represents the rate of change following a fluid particle. Note that if the molecular diffusivity were zero then (3.2) would simply imply that concentration following a fluid particle was constant. (3.1) would then provide all the information needed to predict the evolution of the chemical concentration.

A rough estimate of the magnitude of each of the terms on the right-hand side of the concentration equation (3.2) is given below the equation, assuming that  $U$  is a velocity scale and  $L$  is a length scale. Note that the

ratio of the first (advective) term to the second (molecular diffusive) term is given by dimensionless number, conventionally named the Peclet number

$$Pe = \frac{UL}{\kappa}. \quad (3.3)$$

$Pe \gg 1$  means that diffusion is weak relative to advection. Note that  $Pe$  is the ratio between the time for diffusion over distance  $L$ , equal to  $L^2/\kappa$  divided by the time for advection  $L/U$ .

For the near-surface atmosphere the molecular diffusivity  $\kappa \sim 10^{-5} \text{m}^2 \text{s}^{-1}$ . If we take (for the purposes of argument)  $U = 1 \text{m s}^{-1}$  and  $L = 1 \text{m}$ , this implies that  $Pe \sim 10^5$  or equivalently that the time for diffusion through distance  $L$ ,  $10^5 \text{s}$ , is  $10^5$  times greater than the time for advection through distance  $L$ ,  $1 \text{s}$ . The effects of molecular diffusivity are on this basis expected to be very weak. However the effects of molecular diffusion cannot be neglected entirely, since this would rule out any molecular mixing (so, for example, two species A and B released in different regions of the flow could never come together to react).

A crucial point here is that  $Pe$  depends on the assumed length scale,  $L$  which might be regarded as externally imposed, by the flow geometry, or by the inherent length scales in the flow. But in fact, for the above estimates of terms in equations (3.2) to apply,  $L$  must be the length scale of the concentration field. An important property of many (but not all) fluid flows is that the evolution of the chemical concentration field as predicted by (3.2) tends to reduce systematically the actual length scale of the concentration field,  $l$  say, until the time scale for diffusion is comparable to that for advection. The reduction in scale is achieved by the stirring process, and when  $l$  is small enough for diffusion to be effective the stirring is followed by mixing.

### 3.3. Stretching in linear flows

More precise insight into the stirring process can be obtained by considering a simple model in which the scale of the concentration field is much less than the scale of the velocity field. On the scale of the concentration field the velocity field can be approximated by a Taylor expansion. The first (constant) term may be removed by transforming to a frame of reference moving with the local flow velocity, leaving a velocity field that is a linear function of space,

$$\mathbf{u}(\mathbf{x}, t) \simeq \mathbf{A}(t) \cdot \mathbf{x} \quad (3.4)$$

where  $\mathbf{A}(t)$  is the the local velocity gradient tensor  $\nabla \mathbf{u}$  with components  $\partial u_i / \partial x_j$ . Note that if the flow is incompressible then  $\nabla \cdot \mathbf{u} = 0$  implying that

the trace of the tensor  $\mathbf{A}$  must be zero for each  $t$ . Incompressibility turns out to be a good approximation for atmospheric flows that are important for transport and mixing.

This leads to a simplified evolution equation for a line element  $\mathbf{l}(t)$ , i.e. the line joining two nearby marked points,

$$\frac{d\mathbf{l}}{dt} = \mathbf{A}(t) \cdot \mathbf{l} \quad (3.5)$$

which may be derived from (3.1) by considering two nearby solutions  $\mathbf{X}_1(t)$  and  $\mathbf{X}_2(t) = \mathbf{X}_1(t) + \mathbf{l}(t)$ . The corresponding equation for scalar concentration is that

$$\frac{\partial \chi}{\partial t} + (\mathbf{A}(t) \cdot \mathbf{x}) \cdot \nabla \chi = \kappa \nabla^2 \chi. \quad (3.6)$$

$\mathbf{A}(t)$  is velocity gradient tensor following a fluid particle. It is therefore the time history of this tensor following the flow that determines the stretching process and its coupling to mixing.

Both equations are significant simplifications over their analogues for general flow, but even so solving them for general  $\mathbf{A}(t)$  is not straightforward. It is useful to consider the simplest possible case of two-dimensional flow where the velocity field  $\mathbf{u}$  is a linear function of space  $\mathbf{u} = \mathbf{A} \cdot \mathbf{x}$  with  $\mathbf{A}$  constant in time.  $\nabla u$  is therefore constant in space and time (and is therefore constant following fluid particles). There are three possible sorts of behaviour for these flows, illustrated by the following three examples.

The first is steady 'pure-strain' flow  $\mathbf{u} = (\Gamma x, -\Gamma y)$ , where  $\Gamma$  is constant. Then

$$\mathbf{A} = \begin{pmatrix} \Gamma & 0 \\ 0 & -\Gamma \end{pmatrix}$$

and it follows that the solution of (3.5) is

$$\mathbf{l}(t) = (l_1(t), l_2(t)) = (l_1(0)e^{\Gamma t}, l_2(0)e^{-\Gamma t})$$

. Thus in this case, unless the initial direction of  $\mathbf{l}$  is perfectly aligned with the  $y$ -axis, which is the compression direction for this strain field,  $|\mathbf{l}|$  increases exponentially with  $t$ , and  $\mathbf{l}$  becomes more and more closely aligned with the  $x$ -axis, which the stretching direction.

The second is steady unidirectional shear flow  $\mathbf{u} = (\Lambda y, 0)$  where  $\Lambda$  is constant. Then

$$\mathbf{A} = \begin{pmatrix} 0 & \Lambda \\ 0 & 0 \end{pmatrix}$$

and  $\mathbf{l}(t) = (l_1(t), l_2(t)) = (l_1(0) + l_2(0)\Omega t, l_2(0))$ , implying that  $|\mathbf{l}|$  increases linearly with  $t$ .

A third is the rotational flow  $\mathbf{u} = (-\Omega y, \Omega x)$  where  $\Omega$  is constant. Then

$$\mathbf{A} = \begin{pmatrix} 0 & -\Omega \\ \Omega & 0 \end{pmatrix}$$

and  $\mathbf{l}(t) = (l_1(t), l_2(t)) = (l_1(0) \cos \Omega t - l_2(0) \sin \Omega t, l_2(0) \cos \Omega t + l_1(0) \sin \Omega t)$ , implying that  $|\mathbf{l}|$  stays constant with time – the vector  $\mathbf{l}$  simply rotates at angular velocity  $\Omega$ .

The above three examples illustrate the three possible sorts of behaviour for a line element in a two dimensional flow that is a linear time-independent function of space. In this two-dimensional case the behaviour is determined by  $\det \mathbf{A}$ . If  $\det \mathbf{A} < 0$  then  $\mathbf{l}$  increases exponentially with time, if  $\det \mathbf{A} = 0$  then  $\mathbf{l}$  increases linearly with time and if  $\det \mathbf{A} > 0$  then  $\mathbf{l}$  oscillates with no systematic increase in time. In a corresponding three-dimensional flow there are similar possibilities, though the criteria are more complicated.

Some insight into the case where  $\mathbf{A}$  is time-dependent can be obtained by considering the case of a pure strain that is randomly varying in time – a simple case is where the magnitude of the strain rate is constant, equal to  $\Gamma$ , say, but the axes of strain randomly change direction after a time interval  $\delta$ . The average effect of the stretching over each time interval  $\delta$  may be calculated by noting that the effect is equivalent to that of a strain field with stretching axis in fixed direction, e.g. as considered above, but acting on a line element that is randomly oriented at the beginning of the time interval. If the line element is initially given by  $(\cos \theta, \sin \theta)$  then the effect of the strain field acting over time  $\delta$  is to deform the line element to  $(e^{\Gamma\delta} \cos \theta, e^{-\Gamma\delta} \sin \theta)$ . Anticipating that increase in length will be exponential in time, it is useful to consider the change in  $\log |\mathbf{l}(t)|$  over time  $\delta$  which is given by

$$\log\{|\mathbf{l}(\delta)|/|\mathbf{l}(0)|\} = \frac{1}{2} \log\{e^{2\Gamma\delta} \cos^2 \theta + e^{-2\Gamma\delta} \sin^2 \theta\}. \quad (3.7)$$

The average value of this quantity, obtained by integrating with respect to  $\theta$  from 0 to  $2\pi$  and then dividing by  $2\pi$  is  $\frac{1}{2} \log\{\frac{1}{2}(1 + \cosh 2\Gamma\delta)\}$  and the average rate of stretching  $s$  over many time intervals  $\delta$  is therefore  $s = \frac{1}{2}\delta^{-1} \log\{\frac{1}{2}(1 + \cosh 2\Gamma\delta)\}$ . A key quantity in determining the size of  $s$  is the product  $\Gamma\delta$ . When  $\Gamma\delta \ll 1$ , i.e. the direction of the strain field changes on a time that is much less than the inverse strain rate  $\Gamma^{-1}$ , the above expression reduces to  $s \simeq \frac{1}{2}\Gamma^2\delta = \Gamma \times \frac{1}{2}\Gamma\delta$ .  $s$  is therefore much less than the stretching rate for the steady strain field. When  $\Gamma\delta \gg 1$ , i.e. the

direction of the strain field changes on a time that is much greater than the inverse strain rate  $\Gamma^{-1}$  the corresponding expression is  $s \simeq \Gamma - \delta^{-1} \log 2$ .  $s$  in this case is therefore close to the stretching rate for the steady strain field, but slightly reduced, as a result of the fact that each time the strain field reorients, it takes some time for the line element to align in the stretching direction.

The important point is that for all values of  $\Gamma\delta$  there is exponential stretching, even though the average strain field at any fixed point is apparently zero (in the sense that at the beginning of each time interval  $\delta$  is as likely to be aligned in the compression direction of the strain field as in the stretching direction). The conclusion is that exponential stretching of line elements is something rather robust which does not depend, for example, on steadiness of the strain field. More sophisticated mathematical models of a randomly varying strain field can be formulated, but the general property of all such models is that if the strain has correlation time  $\tau$  and magnitude  $\Gamma$  then the stretching rate  $s \sim \Gamma \min\{\Gamma\tau, 1\}$ . Note, recalling (3.5) for example, that  $\tau$  is the correlation time, of the strain, following a fluid element, sometimes known as the Lagrangian correlation time.

So far we have not mentioned the dynamics of the flow – it is, of course, the dynamics that determines the time evolution of  $\mathbf{A}$ . In a turbulent flow the time evolution might be modelled by a random function – ‘random straining model’ implying exponential increase in length with time. We might conclude that in complex flows exponential stretching is ‘usual’. Cases such as the steady shear flow are ‘unusual’. For ‘most’  $\mathbf{A}(t)$ ,  $|\mathbf{l}(t)|$  increases exponentially with time, i.e. as  $e^{\lambda t}$  where  $\lambda$  may be time-dependent but does not decrease or increase systematically with time. Indeed for a given fluid line element  $\mathbf{l}$  it is useful to define

$$\lambda = \frac{1}{t} \log \left\{ \frac{|\mathbf{l}(t)|}{|\mathbf{l}(0)|} \right\} \quad (3.8)$$

as a measure of stretching rate.

There are of course parts of atmospheric flows where, at least on limited time scales, exponential stretching does not hold and the behaviour is more like the steady shear flow. These include the interior of long-lived coherent eddies (which might be eddies in the turbulent boundary layer or larger-scale flows such as hurricanes or extratropical cyclones) or strong jets (such as the subtropical jet).

### 3.4. The relation between stretching and mixing

To emphasise the implications of material line lengthening and relative dispersion for stirring and mixing, it is useful to consider the evolution of a small material surface (assumed smaller than the length scale on which the velocity field varies) that is initially a sphere (or, in two-dimensions, a small material contour that is initially a circle). The tendency of line elements to stretch implies that the sphere is deformed into an ellipsoid, at least one axis of which systematically increases in time. In an incompressible flow the volume of the sphere remains constant with time, therefore the systematic increase in length of one axis is inevitably accompanied by the systematic decrease in length of another axis. This is a manifestation of the scale reduction that leads to mixing. In a compressible flow there is no absolute constraint on the volume of the sphere, but nonetheless it is the case that in almost all flows the density will not systematically reduce, implying again that one axis must systematically reduce in length. The geometry of the ellipsoidal material surface becomes more complicated when its maximum dimension becomes as large as the length scale on which the velocity field varies. The surface is then strongly distorted and folded as different parts of the surface sample very different velocity gradients.

How is this picture affected by molecular diffusivity? It was noted earlier that the relative size of advective and diffusive terms is  $Pe = UL/\kappa$ . In the local view expressed by (3.6) there is no obvious velocity scale and it is best to consider the typical value,  $S$  of the velocity gradient, implying an alternative definition  $Pe = SL^2/\kappa$  and a length scale  $(\kappa/\lambda)^{1/2}$  above which advection dominates and below which molecular diffusion dominates. Following the picture presented above, a circular patch of tracer of radius  $r_0 \gg (\kappa/\lambda)^{1/2}$  will stretch and thin into an ellipse until its minor axis  $r_0 e^{-\lambda t} \sim (\kappa/\lambda)^{1/2}$ . After this the minor axis decreases no further (since the broadening effect of diffusion is balanced by the narrow effect of continued stretching) but the major axis continues to increase as  $r_0 e^{\lambda t}$ . Since area increases as  $e^{\lambda t}$  the typical tracer concentration must reduce as  $e^{-\lambda t}$  (as patch mixes with its environment). When  $r_0 e^{\lambda t}$  becomes comparable to the length scale on which the velocity field varies the elliptical patch folds back on itself to become a lengthening filament, but the typical width remains as  $(\kappa/\lambda)^{1/2}$ .

The relevance of deformation of material surfaces or curves to the evolution of the concentration of a chemical species is emphasised by noting that a similar picture holds in backward time. Neglecting the effects of diffusiv-

ity for the present, the values of concentration in a small spherical region will be the values that were present in the same material region at the initial time. If that material region is stretched (in backward time) to length scales greater than those on which the concentration varies in the initial condition, then that stretched region, and hence the small spherical region will contain a wide range of different concentration values. It can therefore be safely assumed that the effect of diffusivity will be to homogenize those values over the small spherical region. These complementary views in forward and backward time are pictured schematically in Figure (2). The intimate relation between relative dispersion, i.e. the separation of nearby particles, and mixing has been exploited in many theoretical studies of the mixing problem.

### 3.5. 'Type I' and 'Type II' flows

The stirring and mixing process has so far been described as completely generic. One could equally well be considering the mixing of a smoke plume from a factory into the surrounding boundary layer air, or the mixing into the upper troposphere of boundary layer air that has been lofted in a convective cloud or a convective complex, or the mixing of stratospheric ozone-depleted Antarctic air into mid-latitudes as the polar vortex breaks up in the late spring. These examples range in scales from a hundred metres or so to several thousand kilometres. But the flows that are responsible for stirring and mixing in each of the cases are very different and that has important implications for the stirring and mixing process.

There are two important paradigms for transport and mixing in complex flows. The first, which we might call a 'Type I' flow, is exemplified by three-dimensional turbulent flow. The classical Kolmogorov theory of such flow states that energy is put into system at large scale and is dissipated at small scale. A key parameter, indeed the only externally imposed dimensional parameter is the energy input rate per unit volume  $\epsilon$ . If the energy injection scale is  $L$  and the velocity on that scale is  $U$  then  $\epsilon$  can be estimated as  $\epsilon \sim U^3/L$ . Dimensional analysis implies that at scale  $l$ , the velocity  $u \sim \epsilon^{1/3}l^{1/3}$  and therefore that the velocity gradient, and hence the stretching rate,  $u/l \sim \epsilon^{1/3}l^{-2/3}$ . The stretching rate therefore increases as  $l$  decreases. This implies that the velocity gradient has a complex structure in space and time, and also that the tracer field at scale  $l$  is dominated by the local stretching characteristics of the flow, so that it too has a complex structure in space and time. Note that the Peclet number at scale  $l$ ,  $Pe_l$  say, is estimated to

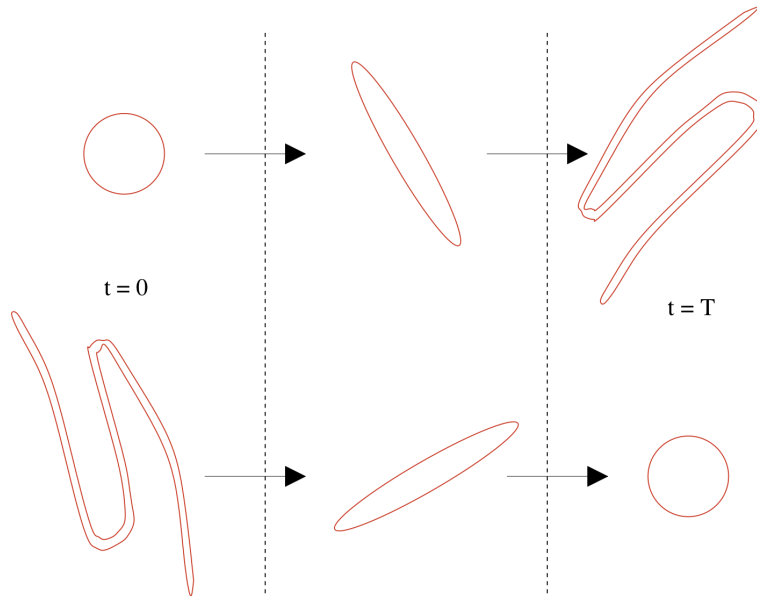


Fig. 2. Schematic of the deformation of two material curves/surfaces. The top panel shows a small circle at time  $t = 0$ , which is then deformed into an ellipse (while its maximum dimension is less than the characteristic scale of the flow) and then into a more complex structure (as different parts of the curve experience very different velocity fields). The bottom panel shows a small circle at time  $t = T$ , which originated from a complex filamental structure at  $t = 0$ . This structure may be obtained by deforming the circle in backward time. The values of chemical concentration inside the circle at  $t = T$  are just those sampled by the filamental structure at time  $t = 0$ . (Note that the two panels do not imply any kind of reversibility – the lower panel corresponds to a particular choice of initial condition that involves into a circle at time  $T$ . If the evolution was continued after time  $T$  the circle would stretch and eventually become geometrically complex, much as in the top panel.)

be  $ul/\kappa \sim \epsilon^{1/3}l^{4/3}/\kappa$  which is  $O(1)$  when  $l \sim \kappa^{3/4}\epsilon^{-1/4}$ , with the latter scale being that on which molecular mixing occurs. (We assume that this scale is no less than the scale at which energy dissipates, which follows if the diffusivity for the tracer is no less than the kinematic viscosity  $\nu$ . This assumption is good for most chemical species in the atmosphere. However it is not good for many common chemical species dissolved in water, so needs to be considered carefully for the ocean.) Now consider the time needed for a tracer structure starting with scale  $L$  to be deformed so that diffusive mixing becomes important. At any scale  $l$  the time to reduce in scale by a factor of 2 can be estimated as  $\epsilon^{-1/3}l^{2/3}$  and the time to the mixing scale is therefore

estimated by  $\epsilon^{-1/3}L^{2/3}(1+2^{-2/3}+2^{-4/3}+\dots+\kappa^{1/2}L^{-2/3}\epsilon-1/6)$ . Since the series is a geometric series and converges as the number of terms increases, this time is relatively insensitive to  $\kappa$  and well estimated by  $\epsilon^{-1/3}L^{2/3}$  which is the eddy turnover time on scale  $L$ . This implies that the time scale for molecular mixing (or 'micromixing') starting with a concentration distribution varying on length scale  $L$  is similar to, i.e. some modest multiple of, the time scale for advective rearrangement of the concentration field, sometimes called 'macromixing' over the length scale  $L$ .

The second type of flow, a 'Type II' flow, has a smooth structure in space and time, so that the velocity gradient also has such a smooth structure. However this does not imply simplicity for particle trajectories. The mathematical theory of dynamical systems, which when applied to particle motion in smooth flows implies the phenomenon of 'chaotic advection', shows that particle trajectories can be very complex. (What is meant by 'chaotic' is that particle trajectories are quasi-random, in other words that the position of a particle at one time gives little information on its position at some future time. Equivalently, nearby particles separately exponentially in time or stretching of material line elements is exponential in time.) Since these flows are smooth, the local velocity gradient and hence local stretching rate, are well estimate by the large scale velocity gradient  $U/L$  where  $U$  and  $L$  are defined as above. In this case the time to stretch by a factor of 2 is independent of scale and the consequence is that the time for a tracer structure to be deformed from the large scale  $L$  to the scale  $(\kappa L/U)^{1/2}$  where molecular diffusion is important is estimated by  $(L/U) \log UL/\kappa$ , i.e. it depends strongly on  $\kappa$ . This implies that the time for 'micromixing' is much larger, by a factor  $(L/U) \log UL/\kappa$ , than the time scale for 'macromixing'. Furthermore, because the velocity gradient is a smooth function of space, the direction of stretched filaments is also a smooth function of space. Since, when the diffusivity  $\kappa$  is small, the filaments will be very thin, this implies that the filaments must be locally unidirectional. (In a 'Type I' flow on the other hand, the velocity gradient, and hence the direction of stretched filaments, varies strongly on small scales.)

In the atmosphere the 'Type I' paradigm applies to the active turbulent regions – the planetary boundary layers and actively convecting regions both in the tropics and the extratropics. The 'Type II' paradigm applies to flows dominated by stable stratification and rotation, i.e. the large-scale flow in the troposphere and stratosphere due to synoptic-scale baroclinic eddies (extratropical cyclones and anticyclones), large-scale waves and non-convecting regions of monsoon circulations and tropical cyclones.

### 3.6. Stirring and transport in quasi-two-dimensional flows

The previous sections have emphasised the importance of the quasi-horizontal large-scale flow, a 'Type-II' flow in long-range atmospheric transport. Therefore it is worth considering simple mathematical models of transport and stirring in such a flow. A convenient idealisation is to consider a two-dimensional and incompressible flow. For such a flow the velocity components  $u$  and  $v$  in the  $x$  and  $y$  directions respectively may be represented in terms of a streamfunction  $\psi(x, y, t)$  as  $u = -\partial\psi/\partial y$  and  $v = \partial\psi/\partial x$ . This might be seen as a model of the flow on an single isentropic surface in the atmosphere – this flow would not be exactly incompressible but the implications for transport and mixing are small.

A first idealisation might be a steady flow, with  $\partial\psi/\partial t = 0$ . For such steady flows the streamfunction  $\psi$  is constant following fluid particles. This puts a very strong constraint on fluid transport – the streamlines – contours of  $\psi$  – are fixed curves and particles can move only along these curves, not across. The streamlines might be regarded as 'transport barriers'. Furthermore in steady flows the stretching of fluid elements, and hence the stirring, is weak, just as the stretching in a linear shear flow was shown to be weak in §3.3. This can be seen, at least for the case of closed streamlines, by the following argument. Consider a line element  $\mathbf{l}(t)$  which at time  $t = 0$  has one end at  $\mathbf{x}_0$ , on the streamline  $\psi(\mathbf{x}) = \Psi$ , and the other end on the neighbouring streamline  $\psi(\mathbf{x}) = \Psi + \delta\Psi$ , implying that  $\mathbf{l}(0) \cdot \nabla\psi(\mathbf{x}_0) = \delta\Psi$ . Now suppose that the time taken for a particle starting on the streamline  $\psi = \Psi$  to move around that streamline once is  $T(\Psi)$ . After this time one end of the line element will have returned to its original position  $\mathbf{x}_0$ . However the other end, on the streamline  $T(\Psi + \delta\Psi)$ , would take  $T(\Psi + \delta\Psi)$  to return, implying that at time  $T(\Psi)$  it is displaced by  $-T'(\Psi)\mathbf{u}(\mathbf{x}_0) = -\mathbf{l}(0) \cdot \nabla\psi(\mathbf{x}_0)T'(\Psi)\mathbf{u}(\mathbf{x}_0)$  from its original position. This displacement is the change in  $\mathbf{l}$  over the time  $T(\Psi)$ . We deduce that  $\mathbf{l}(T(\psi)) = M\mathbf{l}(0)$  where the matrix  $M$  has elements  $M_{ij} = \delta_{ij} - T'(\Psi)u_i(\mathbf{x}_0)\partial\psi/\partial x_j(\mathbf{x}_0)$ . The fact that  $\mathbf{u}(\mathbf{x}_0) \cdot \nabla\psi(\mathbf{x}_0) = 0$  implies that  $(M^n)_{ij} = \delta_{ij} - nT'(\Psi)u_i(\mathbf{x}_0)\partial\psi/\partial x_j(\mathbf{x}_0)$  and hence  $|\mathbf{l}(nT(\Psi))|$  increases only linearly with  $n$ .

If the flow is time dependent, then the strong constraints on particle transport and on stretching are relaxed, since particles no longer remain on a fixed streamline for all time. There have been many studies over the last thirty years or so of the changes in transport and mixing that occur as the a flow changes, through suitable change in one or more parameters,

from a steady flow to one in which there is strong time dependence and the resulting behaviour is described, for example, [11] and [12]. A typical example is where a specified time periodic perturbation is added to a time-independent streamfunction. Studies of these flows are usually 'kinematic' in the sense that no attention is paid to whether the flows are dynamically consistent – the velocity field is simply assumed and the transport and mixing properties investigated.

An example of the changes in transport and mixing as a time-periodic component is added to a steady flow is illustrated in Figure 3. In the underlying steady flow particle trajectories lie along streamlines which are therefore transport barriers. The top panel of Figure 3 shows the streamlines for the example case. Dots and crosses indicate stagnation points, with dots being *elliptic* (a line element centred at this point in the steady flow would rotate but not be stretched systematically) and crosses being *hyperbolic* (a line element centred at this point in the steady flow will be stretched systematically). When a time-periodic perturbation of very small amplitude is added to the steady flow 'most' of the transport barriers corresponding, in the purely steady case, to streamlines are preserved. Between the surviving barriers there are thin regions in which particle trajectories are chaotic and stretching of material line elements is exponential in time, with the thickest regions usually centred on the location of streamlines of the unperturbed flow that pass through hyperbolic stagnation points. This is shown in the middle left hand panel of Figure 3, for  $\epsilon_2 = 0.125$  with  $\epsilon_2$  being the amplitude of the time periodic component. What are shown are 'Poincaré sections' consisting of a large set of points on a given trajectory at time intervals corresponding to the time period of the flow. Three different Poincaré sections, corresponding to three different initial conditions, are shown, as light, middle and dark grey. The light and middle grey sections have the form of single curves and correspond to transport barriers that have been preserved from the steady case. The dark grey section, which includes the hyperbolic stagnation point in the unsteady flow, fills out a finite area and corresponds to a thin mixing region. As the amplitude of the perturbation increases further barriers disappear and mixing regions increase in thickness. Thus in the bottom left-hand panel of Figure 3, for  $\epsilon_2 = 0.025$  the dark grey section, mapping out a single mixing region, has increased in size from  $\epsilon_2 = 0.0125$ , but the light and middle grey sections still correspond to single curves and therefore to barriers. Note in particular that the light grey curve corresponds to a barrier that separates the 'northern' part of the domain from the 'southern' part of the domain. Increasing  $\epsilon_2$

further to 0.05, shown in the middle right-hand panel, suggests a significant change, as the light grey section now fills a finite area and therefore corresponds to a mixing region. The light grey and dark grey mixing regions still appear to be distinct, suggesting that they may be separated by a barrier (which would still in effect divide 'northern' and 'southern' parts of the domain). In fact increasing the length of the calculation shows that there is no absolute barrier, but it is clear that there is nonetheless significant organisation to the transport which inhibits exchange between the 'northern' and 'southern' parts even if it does not prevent it. Finally, as illustrated in the bottom right-hand panel, increasing  $\epsilon_2$  further again, to 0.075, allows rapid exchange between 'northern' and 'southern' parts so that there is a single large mixing region, filled by both light grey and dark grey sections. Figure 3 illustrates this for a particular example of a flow, but the general pattern of behaviour seen here is generic.

Whilst the real large-scale atmospheric flow is certainly not time periodic, it shares some of important features described above. In particular there are apparently strong barriers to transport associated with the subtropical jets, with neighbouring regions of mixing on both poleward and equatorward sides. (See comments on Figure 1.) The precise 'cause-and-effect' relation between jets and transport barriers is subtle. For example in a kinematic model where a systematic jet is added to a simple background eddy field the transport in the cross-jet direction will often be inhibited, i.e. the jet seems to cause the transport barrier. On the other hand, the dynamics of rotating stratified flow is such that the presence of a transport barrier naturally leads to the formation of a jet, i.e. the transport barrier seems to cause the jet. These issues are discussed further in [14] and [15].

#### 4. Modelling approaches

There are many highly developed methods of calculating atmospheric chemical fields. Some of these have been motivated by research, e.g. using such calculations as an aid to interpreting chemical measurements in a field campaign or even as a guide to where and when to take observations, whilst others have been motivated by practical concerns, e.g. predicting the effects of accidental chemical release or establishing the origin of industrial pollutants. Most weather forecasting agencies now provide some kind of air quality forecast and there has already been significant progress towards integrating chemical measurements and chemical model calculations in the same way that meteorological measurements and meteorological models

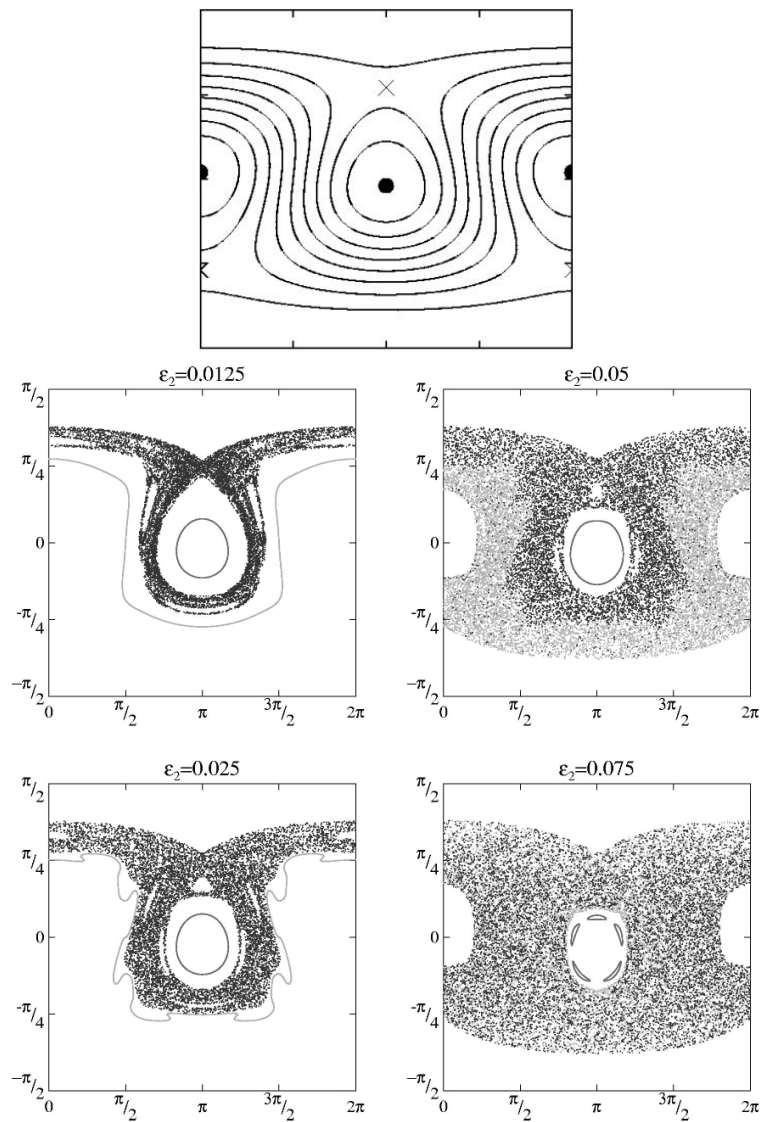


Fig. 3. Reproduced from [13]. Variation of transport and mixing in a simple time-periodic flow on a sphere as the unsteady (time-periodic) component is increased. Top panel: streamlines of the underlying steady flow. Lower panels: Poincaré sections showing points on a given trajectory at time intervals corresponding to the time period of the flow, for different values of  $\epsilon_2$  which is the amplitude of the time periodic component. Three different Poincaré sections, corresponding to three different initial conditions for trajectories, are shown in each case, as light, medium and dark grey. See text for further details and explanation. Copyright 2003 American Institute of Physics. Reproduced by permission of American Institute of Physics.

have been integrated over the last forty years (e.g. see [16]).

The essence of a chemical calculation is to solve the advection-diffusion equation (3.2) for each chemical species, with production and destruction reaction terms on the right-hand side. This first of all requires velocity fields and these may be taken from an observational dataset or else generated by a meteorological numerical model. The former is made possible by the fact that major weather forecasting centres archive global datasets of velocity, temperature and other quantities, which are generated during the forecast process. These datasets are not 'pure' observational data, but are the product of an 'analysis' procedure which finds a best fit of the underlying numerical model to the available data. Part of the reason why this procedure is necessary is that observational data is provided at irregular space and time intervals that cannot straightforwardly be inserted into a meteorological numerical model and neither, of course, could it be straightforwardly be used in a chemical calculation. In the case of velocity fields generated by a meteorological model, the chemical calculation may be 'off-line', meaning that the velocity fields are stored at suitable time intervals during the integration of the meteorological model and then later used for the chemical calculation (the term 'chemical transport model (CTM)' is often used for the associated numerical model with which the chemical calculation is performed), or 'on-line' meaning that the chemical calculations are carried out concurrently with the dynamical calculations required for the meteorological model, which may be a local or global forecast model, or a climate model.

In either 'on-line' or 'off-line' cases the spatial and temporal resolution of the velocity field will typically be 10s to 100km for current global analysis datasets or global numerical models, or 1-10km for local or regional numerical models. In some flows, and certainly in 'Type I' flows where there is an active role for small scales, the effects of these small scales must be represented through 'parametrization', i.e. artificial terms in the model equations which represent the effects of small-scale processes. Again the development of suitable parametrizations has been an important part of the development of meteorological models, for weather forecasting or climate, and for chemical calculations those parametrizations must be adapted, or new parametrizations developed. For example, parametrization of the effects of cumulus convection (which occurs on length scales too small to be represented at all in most models) has been a major effort in meteorological modelling since the associated physical processes, such as transport of water vapour and heating by condensation, play a major role on the larger scale.

Correspondingly over the last ten years or so there has been a major effort to extend cumular parametrizations to include transport of a wider class of chemical species (water vapour is a chemical species, but it is peculiar in that its concentration is strongly limited by temperature) and to include representation of cloud-processing effects such as removal of water-soluble species by precipitation. See e.g. [17] for recent discussion. Of course there are many other processes that need to be included in models, with representation of emissions, either natural or anthropogenic, being particularly important. Again see [5] for a recent review of the broad subject of global and regional air quality including modelling.

In meteorological modelling the dynamical equations are almost invariably solved by Eulerian techniques, where the functions describing the various dynamical quantities are represented on a fixed spatial grid (or there is some equivalent representation such a fixed set of basis functions) and a corresponding approximation to the governing equations is solved. However in solving for chemical fields there remains a genuine choice between the Eulerian approach, based on (3.2), and a Lagrangian approach based on (3.1) to follow the trajectories of air parcels and at the same time solving the chemical equations for the evolution of the concentrations of different species in the air parcel. The Lagrangian approach, at least in its simplest form, regards air parcels as isolated from their surroundings, and therefore implicitly neglects the molecular mixing effects of the diffusive terms on the right-hand side of (3.2). But Eulerian approaches tend to overestimate these mixing effects, essentially because they cannot represent variations in chemical concentrations on scales smaller than the grid scale. As has been discussed in §2, generation of small scales is an essential part of the route to molecular mixing and for the foreseeable future Eulerian models will not be able to resolve the scales at which mixing actually occurs.

Note that parametrizations of unresolved processes can be introduced into the Lagrangian approach just as they can into the Eulerian approach. For example, the effect of small-scale turbulence in the boundary-layer, which in an Eulerian approach might be represented by parametrized flux terms, perhaps augmented diffusive fluxes or some suitable generalization, can in the Lagrangian approach be represented adding random displacements to the trajectories [18]. The same sort of approach can represent encounter with convective clouds [19].

One of the great practical advantages of the Lagrangian approach is simplicity, both practical and conceptual, and this has to be balanced against the artificiality of the 'no mixing assumption'.

## 5. Examples

The following section will describe some examples of recent combined observational and modelling studies of atmospheric chemistry which highlight the different approaches used, both in observation and modelling.

### 5.1. *The 2000 ACTO campaign – combining chemical measurements and backward trajectory calculations (Methven et al 2003)*

The ACTO (Atmospheric Chemistry and Transport) aircraft campaign was based in Prestwick, Scotland, during May 2000. Instruments on a C-130 aircraft of the UK Meteorological Research Flight were used to make measurements to the northwest of Scotland of various meteorological parameters, plus concentrations of chemical species including ozone and carbon monoxide. The Methven et al. paper [20] discusses results from the campaign and gives some nice examples of the sort of work that it is now possible using a combination of chemical data and trajectory calculations based on velocity fields from global meteorological datasets (as described in the previous section).

Figure 4 shows (right-hand panel) satellite measured 'brightness temperature' in the upper troposphere which gives an estimate of water vapour concentrations. Dark colours correspond to dry air, so it can be seen that a filament of dry air runs north-south along the west coast of Scotland, the Irish Sea and south-west England. This dry filament has been drawn out of the lowermost stratosphere, essentially along the 315K (and neighbouring) potential temperature surfaces. (Recall Figure 1.)

The left-hand panel of Figure 4 is a reconstruction of the water vapour concentration on the 383 hPa pressure level, corresponding roughly to the centre of the vertical layer sampled by the satellite instrument. The reconstruction has been performed using a technique known as 'Reverse Domain Filling (RDF) Trajectories'. This technique uses trajectories integrated backwards in time from points distributed across the domain of interest – in this case points distributed in the horizontal on the 383 hPa pressure level. Note that whereas forward trajectory calculations from a region give information on where the air parcels in that region will be transported in future, backward trajectory calculations given information on the origin of those air parcels, i.e. where they have come from in the past. (Recall Figure 2. Reading the top part from left to right corresponds to forward trajectories from the circular region. Reading the bottom part from right

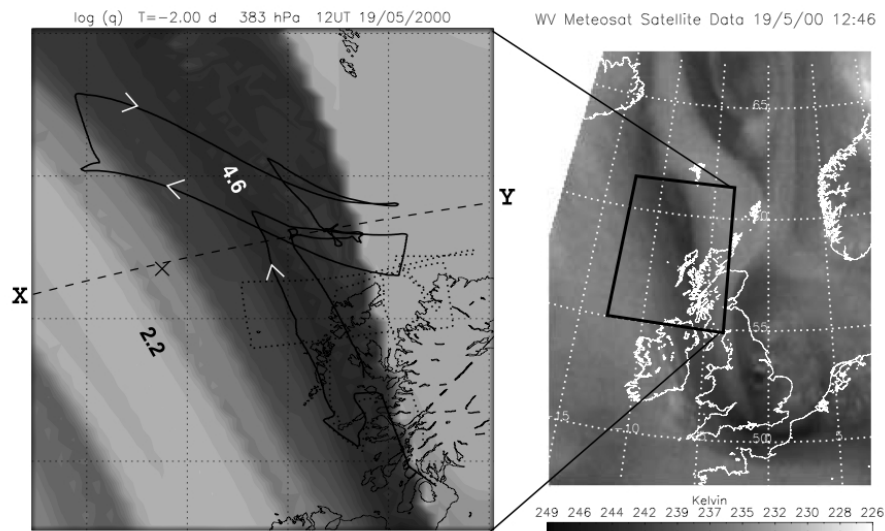


Fig. 4. (From Methven et al 2003.) The right panel shows Meteosat water vapor channel brightness temperature at 12:46 UT, 19 May 2000. Dark shading indicates dry air which originates from the stratosphere (often called a 'dry intrusion'). The left panel shows a RDF3D simulation of specific humidity at 12UT, zooming in on the flight domain. The darkest shading is for  $\log(q) < 4.6$ , the lightest shading is for  $\log(q) > -2.2$ . The bold dotted line is the aircraft flight track, and the bold solid line is the same track shifted to be relative to the air at 12 UT. The arrows show the direction of flight. (The dashed line XY marked a particular great circle section and is not relevant in these notes.) Copyright 2003 American Geophysical Union. Reproduced by permission of American Geophysical Union.

to left corresponds to backward trajectories from the circular region.) A backward trajectory approach therefore allows construction of a field of chemical concentration from the corresponding field known at some earlier time (specifying a suitable initial condition). The value of the concentration at any point is simply determined by following a backward trajectory from that point to the earlier time and then setting the value equal to that of the known concentration field at the position of the backward trajectory at that earlier time. (In practice the known concentration field will be defined on a spatial grid and will therefore have to be interpolated to the position of the backward trajectory which will be unlikely to fall exactly on a grid point.) In the case shown in Figure 4 the relevant chemical species is water vapour and the known concentration field, is taken, just as the velocity fields for the trajectory calculations, from global meteorological analysis datasets, in

this case from the European Centre for Medium Range Weather Forecasting (ECMWF) taken 2 days before the time of the reconstruction. There is close correspondence, in both thickness and orientation, between the observed (right-hand panel) and predicted (left-hand panel), indicating the success of the backward trajectory approach, or more specifically the RDF approach, in this case.

For the case of Type-II flows, the backward trajectory approach potentially gives the possibility of predicting chemical concentration features on length scales that are significantly smaller than either the length scale on which the velocity field is resolved or that on which the initial chemical concentration field are resolved. The former follows because the flow is Type-II and therefore advection and stretching are dominated by large (and therefore resolved) scales. The latter follows on the principle that an initial concentration field may be large-scale (and therefore resolved) and then subsequently deformed by the flow to give much smaller scales (as depicted by the top part of Figure 2). Thus the dry filament shown in Figure 4 might have arisen from deformation over the previous 2 days of a feature that was initially much larger scale. Of course in practice the chemical concentration field at the time at which the initial condition is applied is never completely large-scale. Also the choice of the time at which the initial condition is applied (2 days before the observation for the case shown in Figure 4) is somewhat arbitrary. If the time difference between initial condition and prediction is small then advective effects will be modest and there will not be time for the development of filaments from initially large-scale features. If the time difference is many days then the process of scale-reduction and filamentation shown in the top part of Figure 2 will give a concentration field with strong variation at very small scales. But, in reality the variation in the concentration field at small scales will be limited by molecular diffusion (probably enhanced by the effects of small-scale Type-I three-dimensional turbulent flow). A further difficulty is that small errors in the trajectory calculation imply errors in the position of filamentary structures and the thinner the filament, the more significant these errors appear.

Figure 5 shows selected back trajectories from the region of the aircraft measurements. The trajectories separate in backward time (recall the lower part of Figure 2) suggesting that the air sampled in the measurement regions converged from a large range of locations. In fact from the trajectories three clearly distinct regions can be identified from where this air originated. One region (A) is in the mid-troposphere in Eastern At-

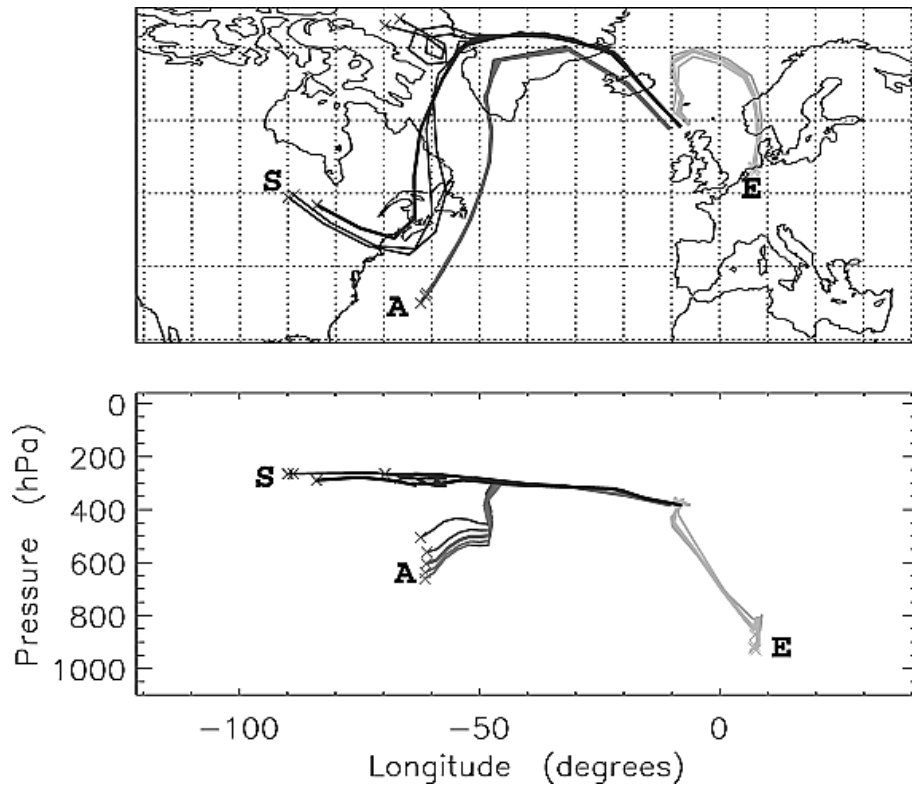


Fig. 5. Reproduced from [20]. Three-day back trajectories from region of observation, shown in longitude-latitude in upper panel and longitude-pressure in lower panel. Copyright 2003 American Geophysical Union. Reproduced by permission of American Geophysical Union.

lantic, another region (S) is the lower stratosphere over central Canada, and another (E), is the lower troposphere over central Europe.

Features corresponding to these different regions of origin can also be clearly identified in Figure 6 which shows time series of measured quantities from one particular flight, together with results from backward trajectory calculations to the points (in space and time) along the flight path. In each panel the thicker line is the measurement and the thinner dashed and solid lines respectively correspond to the backward trajectory reconstruction or to a related 'air-mass average' reconstruction (see [20], for further details) which is based on using potential temperature (more precisely equivalent potential temperature which allows for the effect of latent heating due to

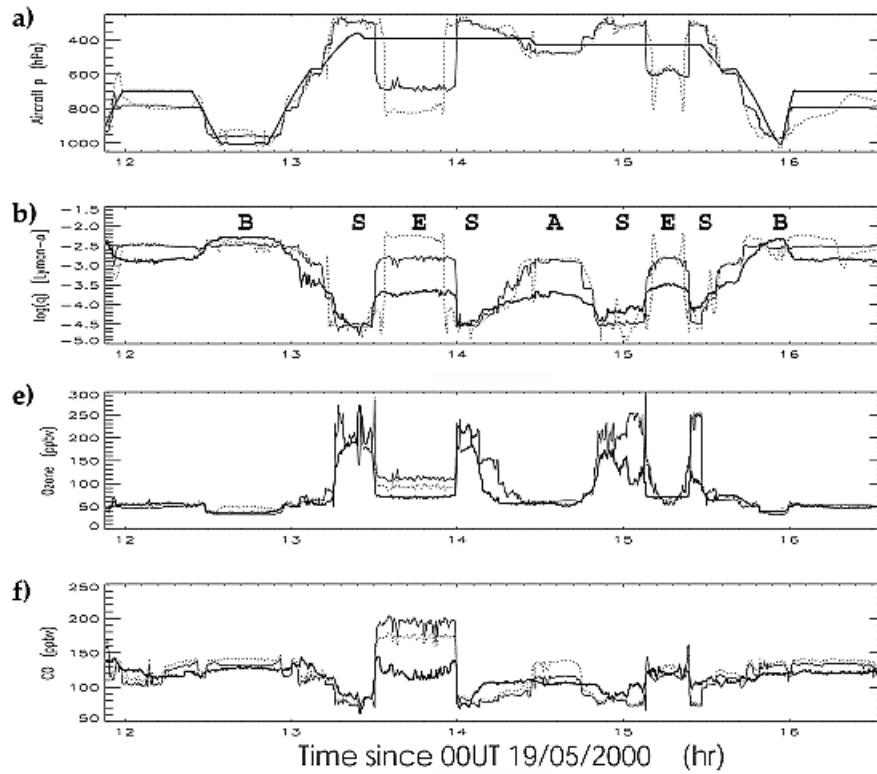


Fig. 6. Reproduced from [20]. Time series of observations (thick lines) along the ACTO flight on 19 May 2000 compared to results from trajectory simulations. (a) Pressure and (b)  $\log(q)$ , where  $q$  is concentration of water in  $\text{g kg}^{-1}$ . Thin dotted lines show values interpolated from global meteorological data to the trajectory origins at 12UT, 17 May 2000. Solid lines show an ‘air-mass average’ of these modeled values. ‘A’, ‘E’ and ‘S’ denote air masses that, according to the back-trajectory calculations, have apparently come from identified source regions (see text). (c) and (d) not shown. (e) Ozone and (f) carbon monoxide concentrations. Dotted line is air-mass average at origin of trajectories. Solid is prediction of chemical model integrated along the trajectory. Copyright 2003 American Geophysical Union. Reproduced by permission of American Geophysical Union.

condensation) and water vapour to specify air mass properties. For (a) pressure and (b) potential temperature the initial condition for the backward trajectory reconstruction comes from ECMWF data. Pressure is, of course, the concentration field of a chemical species and which does not obey equation (3.2), so the ‘reconstructed’ quantity in this case is the pressure 2

days earlier of an air parcel arriving at a given point on the flight track. On the other hand potential does satisfy (3.2), so the 'reconstructed' can be compared directly against the observation. For (e) ozone and (f) carbon monoxide the initial condition comes from an Eulerian global chemical transport model. In this case the thin dotted line shows the back-trajectory prediction and the thin solid line shows the prediction according to a calculation that integrates the chemical reaction equations along the trajectory. The difference between solid and dotted lines in each case therefore corresponds to the amount of chemical production (or destruction if negative) along the trajectory.

Air from each of these regions has a different chemical signature. That from region A is moist and relatively low in ozone ( $O_3$ ) and carbon monoxide (CO). That from region S is dry, high in  $O_3$  and low in CO. That from region E is similar to that from A in that it is moist (both regions are in the troposphere) but different in that it is relatively polluted and therefore high in CO and in  $O_3$  (some of which is likely to have formed through photochemical production as air moves from region E to the region of measurement). Comparison with the detailed chemical fields measured by the aircraft, as shown in Figure 2, shows that the positions and chemical characteristics of the different air masses are generally well predicted by the back trajectory calculation, even, in many cases, down to small-scale features. For example the thin dotted line in (b), the simple back trajectory reconstruction of water vapour concentration, is in qualitative agreement with the measurement, but the filament boundaries are in slightly different locations. This is a manifestation of the displacement error mentioned above. Additionally in the features labelled A and E the predicted water vapour concentration is much larger than the measured concentration. This is because in reality condensation has occurred in these air masses as they have moved towards the measurement point over the previous 2 days. The use of the air-mass average removes these displacement errors, since the predicted quantity is now specified as a function of the measured quantity.

## 5.2. '*Around the world in 17 days*' – *transport of smoke from Russian forest fires (Damoah et al 2004)*'

In May 2003 forest fires in southeast Russia gave rise to smoke plumes which extended very large distances across the northern Hemisphere and were clearly detected by several different satellite instruments. Indeed the plumes, which were advected by the eastward winds in the Northern Hemi-

sphere upper troposphere, could be traced all the way around the globe and back to Scandinavia and Eastern Europe. Whether or not these sorts of plumes from high latitude fires, which can sometimes penetrate the lower stratosphere (Fromm?), have a significant effect on regional-scale chemical distributions is still open to question, but they certainly provide a good opportunity to test modelling skill in atmospheric transport and chemistry. Damoah et al [21] report satellite observations of the May 2003 plumes and show that a numerical model can successfully predicted their evolution over the 17 days or so taken for transport around the globe.

The model used by [21] is a trajectory model (FLEXPART), similar to that used in the Methven et al work [20] reported previously. FLEXPART (e.g. [18]) has been widely used to study many different aspects of atmospheric chemistry and transport. It uses velocity fields from global meteorological analysis datasets. The version used by Damoah et al [21] includes a parametrization of small-scale three-dimensional turbulence, incorporated by adding stochastic fluctuations to the analysis velocity fields, and also a parametrization of convection, incorporated by adding random displacements to the trajectories, with the probability distribution for the displacement set by convective mass fluxes [19]. The smoke plumes in this model are represented by starting trajectories at the locations and times of the fires, with each trajectories representing the path of an air parcel containing a specified mass of carbon monoxide and then defining the smoke distribution at subsequent times by the spatial density of the air parcels. The positions of the fires were detected using the MODIS (Moderate-Resolution Imaging Spectroradiometer) fire product which identifies hot spots. The mass of CO emitted in one day from a hot spot was assumed to be proportional to the area of that hot spot as identified during that day.

Figure 7 shows the total column CO tracer as simulated by the FLEXPART calculation. The left-hand panels shows the results of a calculation based on winds from an ECMWF dataset. The right-hand panels show the results of a corresponding calculation based on winds from the Global Forecast System (GFS) of the National Centre for Environmental Prediction in the US. Generally the two calculations are in good agreement with each other, giving confidence in the wind data which, whilst based on largely the same observational data, is processed completely independently between the two cases. Panel (a) shows that the CO tracer arising from the fires separates into two patches, one of which is advected northwest towards Scandinavia and the other of which is advected eastward over Japan and then further over Canada and back towards northern Europe. It is this sec-

ond patch which is the main focus of attention in [21]. The evolution shown in Figure 7 is, of course, a further demonstration of the stirring and mixing processes described in §3. In this case smoke emissions over a limited spatial region, but for a relatively long time period lead to a large patch of the CO tracer, which is subsequently advected by the large-scale flow. The fact that the tracer reaches regions remote from the source region demonstrates transport, the deformation of the region contain the tracer demonstrates stirring, the fact that the different parts of the initial patch are transported to different locations demonstrates dispersion. The general decrease in peak tracer concentrations and the fact that the region occupied by the tracer appears to increase suggests mixing, but whether or not this mixing is an artificial mixing implied by the FLEXPART approximation to the evolution of a continuously distributed tracer or a real mixing that would be consistent with small-scale observations of the evolving aerosol is harder to tell.

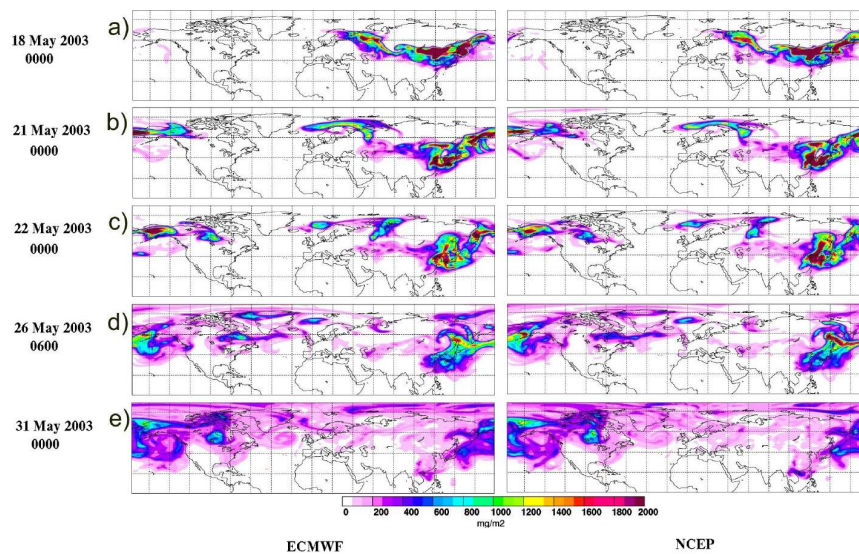


Fig. 7. Reproduced from [21]. Total CO tracer columns from FLEXPART simulations using ECMWF data (left column) and GFS data (right columns) on (a) 18 May 2003 at 00UTC, (b) 21 May at 00 UTC, (c) 22 May at 06 UTC, (d) 26 May at 06UTC and (e) 31 May at 00UTC, respectively. Reproduced by permission of European Geophysical Union.

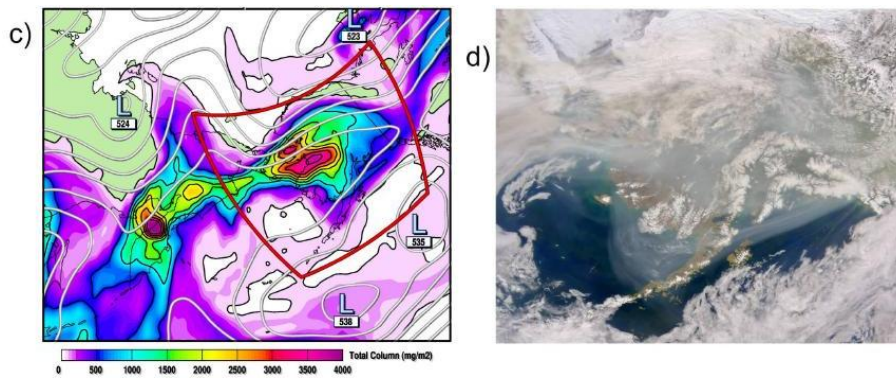


Fig. 8. Reproduced from [21]. (c) FLEXPART ECMWF CO tracer columns over the Bering Sea and adjacent regions with superimposed contours of the 500 hPa geopotential surface, based on GFS analyses, contour interval 5 dam, on 22May 00UTC. Green areas represent land surface, oceans are white. The red rectangle shows approximately the area shown in panel (d); (d) SeaWiFS image showing smoke over Alaska on 21 May; Whitish colors are snow, ice and clouds, whereas the blue-grey indicate smoke. Reproduced by permission of European Geophysical Union.

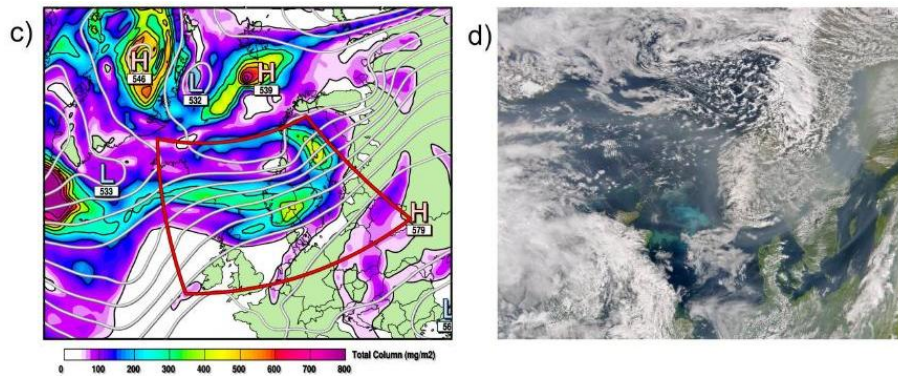


Fig. 9. Reproduced from [21]. (c) FLEXPART ECMWF CO tracer columns over the north-east Atlantic, Europe and Greenland with superimposed contours of the 500 hPa geopotential surface, based on GFS analyses, contour interval 5 dam, at 27 May 15UTC; (d) Image of SeaWiFS sensor showing smoke over Scandinavia on 27 May, 2003 at 12:54 UTC. Reproduced by permission of European Geophysical Union.

More detail is shown in Figures 8 and 9 which show both the calculated

CO tracer, using ECMWF winds, and also images from the Sea-viewing Wide Field-of-View Sensor (SeaWiFS) instrument on the SeaStar satellite, which detects aerosol (i.e. smoke particles in this case). Both more detail is shown in Figures 8 and 9 show rather good agreement between the calculated CO tracer and the SeaWiFS aerosol. In Figure 8 there is a large region of aerosol over western Alaska, including the Aleutians. In Figure 9 there is aerosol extending from the North Sea across Denmark and into the rest of Scandinavia. The conclusion here is that the FLEXPART model has significant skill in predicting the spread of the aerosol over many thousands of kilometers and over a period of several days.

### 5.3. *'Observational and modeling analysis of a severe air pollution episode in western Hong Kong' (Fung et al 2005)*

This third example is concerned with a severe air pollution episode in the western part of Hong Kong in late December 1999 [22]. Consistent with the emphasis elsewhere in these lecture notes, [22] argue that this episode was not due to emissions within Hong Kong itself, but due to biomass burning about 100km to the east.

Figure 10 shows concentration of nitrogen dioxide  $\text{NO}_2$  at two different observing stations in Hong Kong. The solid line shows Tung Chung station which is in western Hong Kong, in an open area on the outskirts of the territory. The dashed line shows Causeway Bay station, which is in the most densely occupied central urban area. It is therefore not surprising that nitrogen dioxide concentrations at Tung Chung are generally lower than those at Causeway Bay. However Figure 10 shows that for periods during the 28th December to 31st December period nitrogen dioxide concentrations at Tung Chung significantly exceed those at Causeway Bay, and indeed exceed those observed at Causeway Bay at any time during the 8-day period shown. Peak concentrations at Tung Chung are considerably greater than values considered to be potentially harmful to human health.

Fung et al [22] use a variety of evidence to argue that the high levels of  $\text{NO}_2$  observed at Tung Chung result not from local emissions but from burning of vegetation in a region about 100km to the north of Hong Kong. This includes information on the chemical composition of the polluted air, but the most straightforward are satellite images which show the presence of fires and the resulting smoke and haze which extends across the western half of Hong Kong, where Tung Chung is located, but which is much less

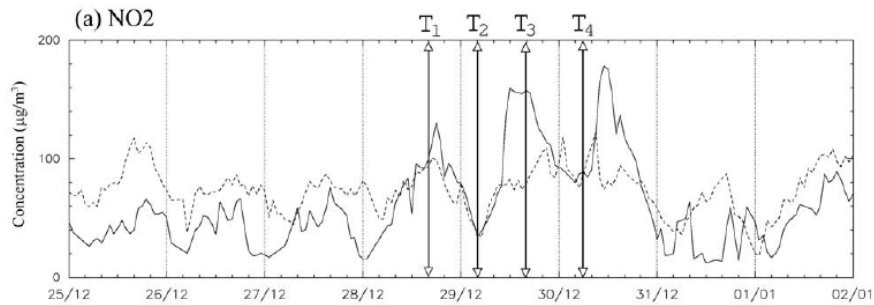


Fig. 10. Reproduced from [22]. Concentration of nitrogen dioxide ( $\text{NO}_2$ ) at Tung Chung station (solid line) and Causeway Bay station (dashed line) from 25 December 1999 to 2 January 2000. The pollution episode which lasted for three consecutive days (28-30 December 1999) falls during the middle of this period. Daily highs and lows of  $\text{NO}_2$  concentration during the episode are indicated by times  $T_i$  ( $i = 1, 2, 3, 4$ ). Note that  $T_1$  corresponds to panel (b),  $T_2$  to panel (c), and  $T_3$  approximately to panel (d) of Figure 11. Copyright 2005 American Geophysical Union. Reproduced by permission of American Geophysical Union.

apparent over the eastern part where Causeway Bay is located.

The previous sections, §5.1 and §5.2, have discussed successful application of transport calculation based on wind fields from large scale meteorological datasets. An important point made in [22] is that when considering local variation in pollutant concentration in a region of complex topography such as Hong Kong, the usefulness of transport calculations will be strongly limited by the spatial and temporal resolution of the wind field, and that provided by the large-scale meteorological datasets is unlikely to be sufficient. Therefore the approach taken in [22] is to use velocity fields predicted by a regional-scale meteorological model to drive a particle-based transport calculation. The regional-scale model is based on a set of four nested domains, with the spatial resolution becoming finer from the outermost domain to the innermost (varying from a horizontal grid size of 40.5 km for the outermost domain to 1.5 km for the innermost domain). Even for the innermost domain it is accepted that turbulent velocity fluctuations at unresolved scales are potentially important and the effect of these is represented by adding random fluctuations to the velocity field used to advect the particles. (This approach is well-developed for 'Type I' turbulence which is what is being represented here.) The parameters for the random fluctuations are set in part by the predicted characteristics of the sub-grid-scale

parametrised turbulence in the meteorological model.

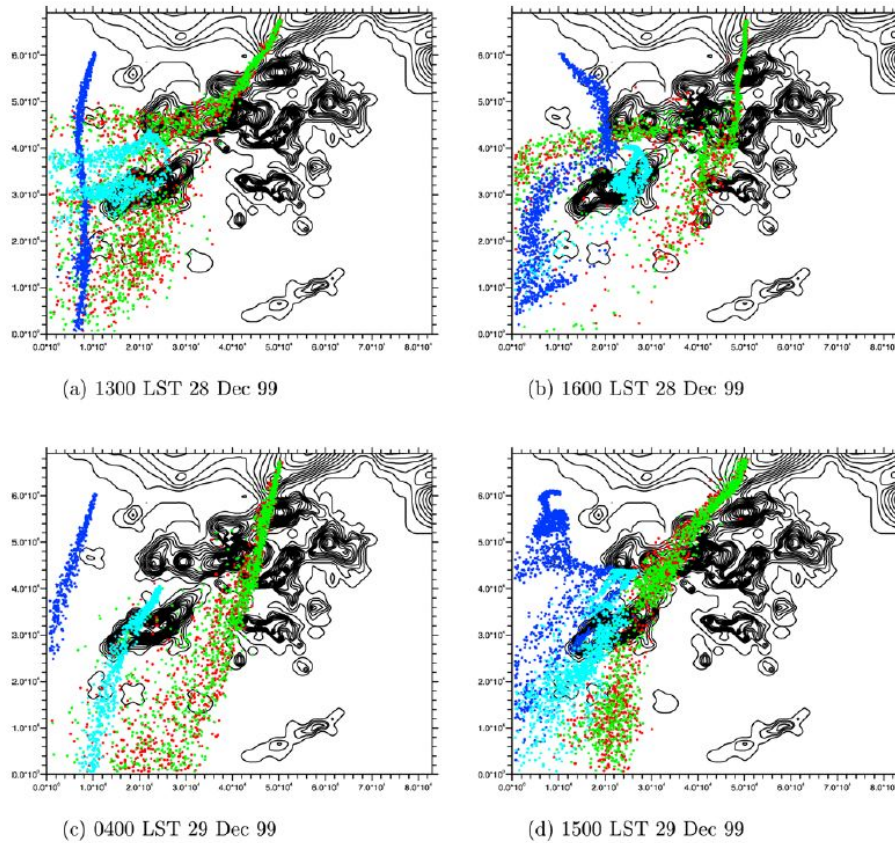


Fig. 11. Reproduced from [22]. Tracer plumes, indicated by particle positions, at different times during the pollution episode. (See text for further details.) The contours correspond to topographic height. Tick marks on  $x$  and  $y$  axes are at intervals of 1 km. Copyright 2003 American Geophysical Union. Reproduced by permission of American Geophysical Union.

Figure 11 shows calculated distributions of particles released in four different locations. The red and green particles are respectively released at 100m and 200m in the region to the north of Hong Kong where the fires occurred. The light and dark blue particles on the other hand are released to the west of Hong Kong to highlight the existence of a convergence region in

the horizontal flow, which is argued to favour trapping of pollutant species and therefore to contribute to the large concentrations observed at Tung Chung. Panels (a), (b) and (d) show daytime conditions where the complex pattern of the blue particles reveals the complicated circulation caused by land-sea contrasts and topographic effects. Other diagnostics show that at these times there is transport of pollutant downwards of pollutant species from the top of the planetary boundary layer. At night time on the other hand, shown in panel (c) the pattern of circulation is much simpler and the red and green particles are simply advected to the south and south-west without any tendency for trapping.

The study in [22] therefore shows convincingly that remote sources of pollution can be very important for air quality in urban areas, but also that, particularly in a region such as Hong Kong, that local details of the flow must be included in any transport calculation in order to capture the spatial and temporal variations in concentration of pollutant species.

## 6. Conclusion

There are many different aspects of atmospheric physics and chemistry that are relevant to understanding and predicting air quality. These notes have focussed on the fluid dynamics of transport and mixing, in particular, while giving an impression of how this topic relates to the broader question of how to use atmospheric models to understanding observations and to make useful predictions. The reader is reminded of [3] and [5] as articles that give a much broader perspective.

It is certainly the case that, whilst in the past weather forecasting and climate prediction on the one hand and air quality on the other have been regarded as separate issues, the strong relation between them is now accepted. Therefore (e.g. see [5]) it needs to be accepted that future strategies for minimising climate impact, e.g. by reducing emissions of long-lived greenhouse gases, and or for improving air quality, e.g. by changing engine technology, need to be considered together, since there are trade-offs – some options that are beneficial for one are adverse for the other. It is also the case that prediction of future air quality not only needs to take account of likely changes in emissions, but also the fact that those emissions are into a background atmosphere that is different from our current atmosphere. Finally some aspects of climate change themselves have air quality implications. These include, for example, the possibility of more summer heatwaves. A study of the effects of the 2003 European heatwave over the

UK [23] suggests that, not only did the associated anticyclonic circulation and elevated temperatures lead to high values of ozone from remote sources, but also that increased emissions of ozone precursors from vegetation as a result of the high temperatures might also have significantly enhanced local ozone concentrations. Another larger-scale effect might be that the effects of climate change on the coupled troposphere-stratosphere system are such that the transport of ozone from stratosphere to troposphere increases, implying an increase in background concentrations of ozone in the troposphere [24]. This means that the maximum concentrations ozone arising in polluted regions will also typically increase and therefore, potentially, that concentrations regarded as potential harmful to health will be encountered more frequently.

### Acknowledgments

This article is based on lectures given by the author at the Spring School on Fluid Mechanics and Geophysics of Environmental Hazards held during the period 19 April to 2 May 2009 at the IMS of the National University of Singapore. The author thanks IMS for hospitality and the students at the School for their enthusiasm and interest.

### References

1. M. Amann, D. Derwent, B. Forsberg, O. Hänninen, F. Hurley, M. Krzyzanowski, F. de Leeuw, S.J. Liu, C. Mandin, J. Schneider, P. Schwarze and D. Simpson, *Health risks of ozone from long-range transboundary air pollution*, World Health Organization Regional Office for Europe, Copenhagen, 2008. (Available from <http://www.euro.who.int>)
2. Royal Society, *Ground-level ozone in the 21st century*. Policy Document 15/08. The Royal Society, London, 2008. (Downloadable from <http://royalsociety.org>)
3. H. Akimoto, “Global air quality and pollution”, *Science*, 302, pp. 1716-1719, 2003.
4. R.G. Derwent, P.G. Simmonds, S. O’Doherty, D.S. Stevenson, W.J. Collins, M.G. Sanderson, C.E. Johnson, F. Dentener, J. Cofala, R. Mechler and M. Amann., “External influences on Europe’s air quality: baseline methane, carbon monoxide and ozone from 1990 to 2030 at Mace Head, Ireland”, *Atmospheric Environment*, 40, pp. 844-855, 2006.
5. P.S. Monks and 62 co-authors, “Atmospheric composition change global and regional air quality”, *Atmospheric Environment*, 43, 5268-5350, 2009.
6. J.T. Houghton, *The Physics of Atmospheres*, Cambridge University Press, 320pp, 3rd Edition, 2002.

7. J.R. Holton, *An Introduction to Dynamical Meteorology*, Academic Press, 535pp, 4th Edition, 2004.
8. G.K. Vallis, *Atmospheric and Oceanic Fluid Dynamics*, Cambridge University Press, 745pp, 2006.
9. R.E. Newell, V. Thouret, J.Y.N. Cho, P. Stoller, A. Marengo and H.G. Smit, "Ubiquity of quasi-horizontal layers in the troposphere", *Nature*, pp. 316-319.
10. J.R. Holton, P.H. Haynes, M.E. McIntyre, A.R. Douglass, R.B. Rood and L. Pfister, "Stratosphere-troposphere exchange", *Reviews Geophysics*, 33, pp. 403-439, 1995.
11. J.D. Meiss, "Symplectic maps, variational principles and transport", *Reviews of Modern Physics*, 64, pp. 795-848, 1992.
12. S. Wiggins, *Chaotic transport in dynamical systems*. Springer-Verlag, 301pp, 1992.
13. E. Shuckburgh and P. Haynes, "Diagnosing transport and mixing using a tracer-based coordinate system", *Physics of Fluids*, 15, pp. 3342-3357, 2003.
14. P.H. Haynes, D.A. Poet and E.F. Shuckburgh, "Transport and Mixing in Kinematic and Dynamically Consistent Flows", *Journal of Atmospheric Sciences*, 64, pp. 3640-3651, 2007.
15. D.G. Dritschel and M.E. McIntyre, "Multiple Jets as PV Staircases: The Phillips Effect and the Resilience of Eddy-Transport Barriers", *Journal of Atmospheric Sciences*, 65, pp. 855-873, 2008.
16. A.J. Geer, W.A. Lahoz, S. Bekki, N. Bormann, Q. Errera, H.J. Eskes, D. Fonteyn, D.R. Jackson, M.N. Juckes, S. Massart, V.-H. Peuch, S. Rharmili and A. Segers, "The ASSET intercomparison of ozone analyses: method and first results", *Atmospheric Chemistry and Physics*, 6, 5445-5474, 2006.
17. H. Tost, M.G. Lawrence, C. Bruehl, P. Joeckel, the GABRIEL team and the SCOUT-O3-DARWIN/ACTIVE team, "Uncertainties in atmospheric chemistry modelling due to convection parameterisations and subsequent scavenging", *Atmospheric Chemistry and Physics*, 4, 1931-1951, 2010.
18. . A. Stohl, C. Forster, A. Frank, P. Seibert, and C. Wotawa, "Technical note: The Lagrangian particle dispersion model FLEXPART version 6.2", *Atmospheric Chemistry and Physics* 5, 24612474, 2005.
19. C. Forster, A. Stohl and P. Seibert, "Parameterization of Convective Transport in a Lagrangian Particle Dispersion Model and Its Evaluation", *Journal of Applied Meteorology and Climatology*, 46, pp. 403-422, 2007.
20. J. Methven, S. R. Arnold, F. M. O'Connor, H. Barjat, K. Dewey, J. Kent and N. Brough, "Estimating photochemically produced ozone throughout a domain using flight data and Lagrangian model", *Journal of Geophysical Research*, 108, 4721, 2003.
21. R. Damoah, N. Spichtinger, C. Forster, P. James, I. Mattis, U. Wandinger, S. Beirle, T. Wagner and A. Stohl, "Around the world in 17 days – hemispheric transport of forest fire smoke from Russia in May 2003", *Atmospheric Chemistry and Physics*, 4, pp. 1311-1321, 2004.
22. J. C. H. Fung, A. K. H. Lau, J. S. L. Lam and Z. Yuan, "Observational and modeling analysis of a severe air pollution episode in western Hong Kong", *Journal of Geophysical Research*, 110, D09105, 2005.

23. J. D. Lee and 26 coauthors, “Ozone photochemistry and elevated isoprene during the UK heatwave of August 2003”, *Atmospheric Environment*, 40, pp. 7598-7613, 2006.
24. G. Zeng and J. A. Pyle, “Changes in tropospheric ozone between 2000 and 2100 modeled in a chemistry-climate model”, *Geophysical Research Letters*, 30, 1392, 2003.